

ARTICLE

Received 11 Oct 2013 | Accepted 28 Mar 2014 | Published 2 May 2014

DOI: 10.1038/ncomms4754

OPEN

Coaxial wet-spun yarn supercapacitors for high-energy density and safe wearable electronics

Liang Kou¹, Tieqi Huang¹, Bingna Zheng¹, Yi Han¹, Xiaoli Zhao¹, Karthikeyan Gopalsamy¹, Haiyan Sun¹ & Chao Gao¹

Yarn supercapacitors have great potential in future portable and wearable electronics because of their tiny volume, flexibility and weavability. However, low-energy density limits their development in the area of wearable high-energy density devices. How to enhance their energy densities while retaining their high-power densities is a critical challenge for yarn supercapacitor development. Here we propose a coaxial wet-spinning assembly approach to continuously spin polyelectrolyte-wrapped graphene/carbon nanotube core-sheath fibres, which are used directly as safe electrodes to assembly two-ply yarn supercapacitors. The yarn supercapacitors using liquid and solid electrolytes show ultra-high capacitances of 269 and 177 mF cm⁻² and energy densities of 5.91 and 3.84 μWh cm⁻², respectively. A cloth supercapacitor superior to commercial capacitor is further interwoven from two individual 40-cm-long coaxial fibres. The combination of scalable coaxial wet-spinning technology and excellent performance of yarn supercapacitors paves the way to wearable and safe electronics.

¹MOE Key Laboratory of Macromolecular Synthesis and Functionalization, Department of Polymer Science and Engineering, Zhejiang University, 38 Zheda Road, Hangzhou 310027, China. Correspondence and requests for materials should be addressed to C.G. (email: chaogao@zju.edu.cn).

Supercapacitors are featured by the fast charge/discharge capacity, long lifecycle, wide range of operating temperatures and safety, which have been widely applied in the fields of digital cameras, mobile phones, electrical tools and pulse laser techniques^{1,2}. Yarn supercapacitors (YSCs) are of particular interest because of their merits of tiny volume, high flexibility and weavability, and are promising for the next generation of wearable electronic devices^{3,4}. Compared with batteries, supercapacitors show much lower-energy density, limiting their practical applications. Therefore, it is crucial to enhance their energy densities (E) while retaining their intrinsic high specific power densities (P) for the development of YSCs. Increasing the charge-storage capability and decreasing the volume of YSCs are two main approaches to enhance E . To improve the charge-storage capability of YSCs, conductive carbon materials with high specific area such as carbon fibre⁴, fibres of carbon nanotubes (CNTs)⁵, graphene^{3,6} and ordered mesoporous carbon⁷ were commonly selected as electrodes, and electrical-active materials with faradaic pseudocapacitance such as metal oxides (for example, MnO_2)⁸ and conducting polymers (for example, polypyrrole⁹, polyaniline (PANI)⁵, and poly(3,4-ethylenedioxythiophene, PEDOT)¹⁰) were tried to incorporate into/on the electrodes. The capacitance (C) of YSCs was then enhanced from 2.4 to 86.8 mF cm^{-2} in the past 3 years^{4,11}; however, the C and E values are still quite low for practical applications. Alternatively, decreasing the YSC volume shall be an effective way to increase volumetric E , yet it has a high risk of short circuit of electrodes.

To date, all of the as-prepared fibres used for fabricating YSCs are naked, and thus are easy to be short-circuited when they are close to each other^{3,5}. Although post-coating a layer of poly(vinyl alcohol) (PVA) solid electrolyte partly reduces the probability of short circuit, the coating process is complicated and time-consuming, and it is hard to evenly coat the PVA layer. The resultant YSCs showed unsatisfied C and low E ⁶. Therefore, it is still a big challenge to develop a simple yet effective approach to directly prepare sheath-protected fibre electrodes with ultra-high C and E .

In this work, a coaxial wet-spinning assembly strategy is proposed to readily prepare polyelectrolyte-wrapped carbon nanomaterial (for example, graphene, CNTs and their mixture) core-sheath fibres that are applied directly as contactable and interweaving YSC electrodes without the risk of short circuit. The resulting compact two-ply YSCs show high C and E values up to 177 mF cm^{-2} (158 F cm^{-3}) and $3.84 \mu\text{Wh cm}^{-2}$ (3.5 mWh cm^{-3}), respectively. C and E are further improved to 269 mF cm^{-2} (239 F cm^{-3}) and $5.91 \mu\text{Wh cm}^{-2}$ (5.26 mWh cm^{-3}) using liquid electrolyte. For the first time, a cloth supercapacitor with C higher than commercial capacitor is interwoven from two individual ultra-long (40 cm) continuous coaxial fibres. The combination of industrially viable coaxial wet-spinning assembly approach and ultra-high electrochemical performance of YSCs paves the way to wearable and safe electronics.

Results

Coaxial wet-spinning assembly approach to polyelectrolyte-wrapped graphene fibres. Our group has first demonstrated that continuous graphene fibres could be achieved by wet-spinning graphene oxide (GO) liquid crystals (LCs)^{12,13} followed by chemical reduction^{14,15}, opening the door to macroscopic, multi-functional graphene fibres with widely potential applications including in the area of YSCs⁶. Recently, other groups also confirmed the fabrication of graphene fibres by either wet-spinning technology^{16–19} or dimensionally confined hydrothermal strategy²⁰. The wet-spinning assembly approach was also successfully extended to create porous aerogel fibres²¹,

hollow graphene fibres²² and nacre-mimetic graphene/polymer composite fibres^{15,23,24}. The resulting graphene fibres are lightweight, electrically conductive, strong, flexible and chemical-resistant, which is promising for practical applications in multifunctional textiles and wearable electronics. However, despite these efforts in the fabrication of various structural fibres, all of them are also naked with the risk of short circuit when used as electrodes, which is unfavourable for the construction of safe electronics such as YSCs.

To solve this problem, we designed a coaxial wet-spinning assembly strategy to prepare polyelectrolyte-wrapped graphene fibres. Although coaxial electrospinning technology has been utilized to spin core-sheath nanofibres²⁵, coaxial wet-spinning approach has never been established to prepare coaxial microfibres from colloidal nanoparticles because of the extreme difficulty for the selection of desirable coagulation bath as well as harmonious solvents of inner and outer components. Figure 1a shows the schematic illustration of our coaxial wet-spinning process (the photograph of corresponding equipment is shown in Supplementary Fig. 1). The spinneret is featured by two inlets that connect the inner and outer channels, respectively. We first selected the aqueous GO LC as the inner spinning dope since it was easily spun into continuous microfibres according to the established wet-spinning assembly protocol. The aqueous solution of sodium carboxymethyl cellulose (CMC) was chosen as the outer spinning dope because CMC is an ionically conductive while electrically insulative polyelectrolyte. Such a polymer sheath ensures fibre electrodes free of short circuit when intertwined together, while allowing ions to smoothly penetrate from the electrolyte matrix to electrodes simultaneously.

Typically, the aqueous GO LC from the inner channel and the CMC aqueous solution from the outer channel were synchronously injected into the coagulating bath of ethanol/water (5:1 v/v) solution with 5 wt% CaCl_2 (ref. 13). Wet CMC-wrapped GO coaxial fibres (GO@CMC) were then shaped rapidly (Fig. 1b), and the magnified photograph (Fig. 1c) showed clear core-sheath structure as designed. The GO dispersions were prepared according to the previous protocol^{15,26,27}. Atomic force microscopy demonstrates that GO is a monolayer with the thickness of 0.7 nm (Supplementary Fig. 2). Scanning electron microscopy (SEM) images also prove the fine dispersity of GO sheets since no aggregation was observed (Supplementary Fig. 3). The solidification process of GO@CMC fibre was *in situ* traced using polarized-light optical microscopy. Vivid schlieren texture was found for the core part of GO because of its LC birefringence (Fig. 1d). During the solidification process, the bright texture was maintained, indicating the uniform alignment of GO sheets along the fibre axis in the shrinkage process (Supplementary Fig. 4). At the same time, the outer black polymer sheath without birefringence was well retained until full solidification, demonstrating the continuous core-sheath structure of GO@CMC fibre (Supplementary Fig. 4).

The GO@CMC fibres were chemically reduced by hydroiodic acid¹⁴. The colour of the core was then changed from brown (Fig. 1b,c) to dark while the polyelectrolyte sheath retained well (Fig. 1e–g). The chemically reduced GO@CMC fibres (RGO@CMC) were highly conductive with a conductivity of $\sim 7,000 \text{ S m}^{-1}$ as measured from their naked ends of the core. Such a high conductivity is comparable to that of neat graphene fibres and papers ($\sim 7,000\text{--}25,000 \text{ S m}^{-1}$), confirming the integrity of the inner fibre and thus enabling it to be used as an electrode of YSCs. On the contrary, the whole fibre was electrically insulative as measured from its side face because of the protection of the insulative polymer sheath (Supplementary Fig. 5). Such well-defined sectorization of core-sheath fibre paves the way to safe assembly of microelectronics. Similar to the wet-spinning of

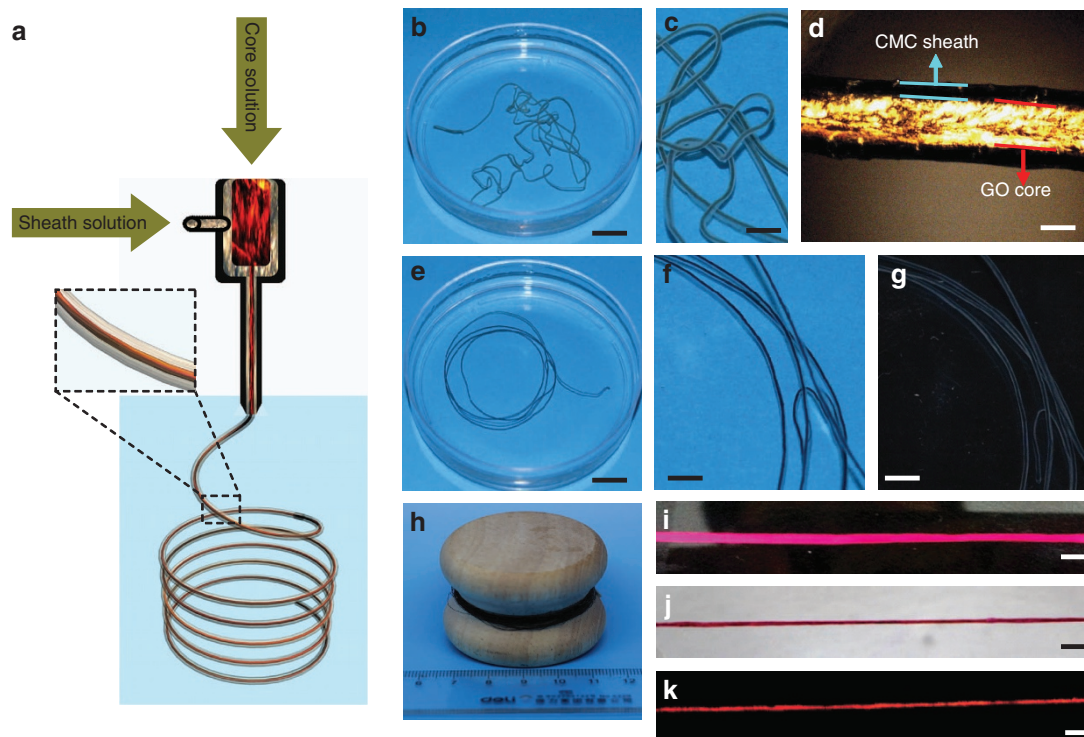


Figure 1 | Coaxial wet-spinning assembly process and the as-prepared core-sheath fibres. (a) Schematic illustration showing the coaxial spinning process. (b) A single intact wet GO@CMC fibre and its magnified image (c). (d) Polarized-light optical microscopy image of wet GO@CMC fibre indicating the core-sheath structure and the well-aligned GO sheets in the core part. (e) A wet RGO@CMC fibre and its magnified images with blue (f) and black (g) backgrounds. (h) The macroscopic photo of the RGO@CMC coaxial fibres. Wet (i) and dry (j) coaxial fibres dyed by rhodamine B and its fluorescence photos (k) in the dark under UV irradiation. Scale bars, 1 cm (b,e), 5 mm (c,f,g), 100 μm (d) and 2 mm (i-k).

neat graphene fibres, continuous GO@CMC fibres were obtained by the coaxial wet-spinning approach, as shown in Supplementary Movie 1. Consequently, ultra-long coaxial fibres up to 100 m were achieved (Fig. 1h), showing large-scale productivity of the multifunctional core-sheath fibres. In addition, the CMC sheath was swollen in ethanol/water (3:1 v/v) solution to colour the fibres with dyes such as rhodamine B, rendering the fibres colourful (Fig. 1i,j) and fluorescence-emissive (Fig. 1k).

The microscopic morphology of the coaxial fibres was characterized using SEM. Figure 2a–c shows typical SEM images of a GO@CMC fibre with a GO core of *ca.* 50 μm and a CMC sheath of *ca.* 25 μm thickness. The GO core is featured by the compact layered structures with dentate bends, which is similar to the oriented structures of neat graphene fibres¹³. The CMC sheath wraps the core tightly without any gaps and voids, which is extremely important for the ion transport when served as supercapacitor electrodes, as evidenced by transmission electron microscopy (TEM) images in Supplementary Fig. 6. Diameter of the GO core and thickness of the CMC sheath were readily adjusted by changing either the concentration or outflow velocity of GO and CMC spinning dopes (Fig. 2d–f and Supplementary Fig. 7). After the chemical reduction by hydroiodic acid, the layered structure of core becomes slightly fluffy and cellular (Fig. 2g–i), which could largely increase the accessible area of electrolyte. The coaxial fibres showed ultra-high flexibility with elongation of 8–10% and good mechanical strength (73–116 MPa; Supplementary Fig. 8). This robustness is propitious to their use in woven devices.

Extension of coaxial wet-spinning assembly approach. Besides graphene, CNTs were also widely used as electrically conductive

electrodes. Two main protocols have been developed to make macroscopic CNT fibres: dry drawing of aligned CNTs⁵ and wet-spinning of surfactant-stabilized CNTs with a coagulation bath of PVA aqueous solution²⁸. However, it is still hard to directly wet-spin neat CNTs in the absence of surfactants or polymers because of their relatively poor dispersibility. In this paper, we realized the continuous wet-spinning of neat CNTs via the as-established coaxial spinning assembly approach (Supplementary Movie 2). Likewise, as the inner component of CNT dispersions was co-injected with the outer component of CMC dope into the coagulation bath, continuous CMC-wrapped CNT fibres (CNT@CMC) were produced. This process is similar to the coaxial electrospinning of nanoparticles without spinnability²⁵. Figure 2j–l shows typical features of CNT@CMC fibres. The thickness of the sheath is 2–5 μm and the diameter of the CNT core is *ca.* 50 μm . The CNT core is compact without any voids, and the CNTs are also oriented along the fibre axis because of the shear stress of wet-spinning in the spinneret capillary.

We further extended the coaxial wet-spinning assembly approach to prepare continuous coaxial fibres with the core of mixture of RGO and CNTs, denoted as RGO + CNT@CMC (Fig. 2m–o). CNTs were coated on the surfaces of RGO densely and separated the adjacent RGO sheets aligned with layered structures (Fig. 2o). The coating of CNTs on RGO sheets greatly increases the specific area of the fibres, which is beneficial to energy storage when used as YSC electrodes. Moreover, replacing the outer layer of CMC by GO dispersion, we also prepared all-carbon RGO + CNT@RGO core-sheath fibres (Supplementary Fig. 9). Therefore, our coaxial wet-spinning assembly strategy is universal and versatile to create designed, multifunctional core-sheath fibres.

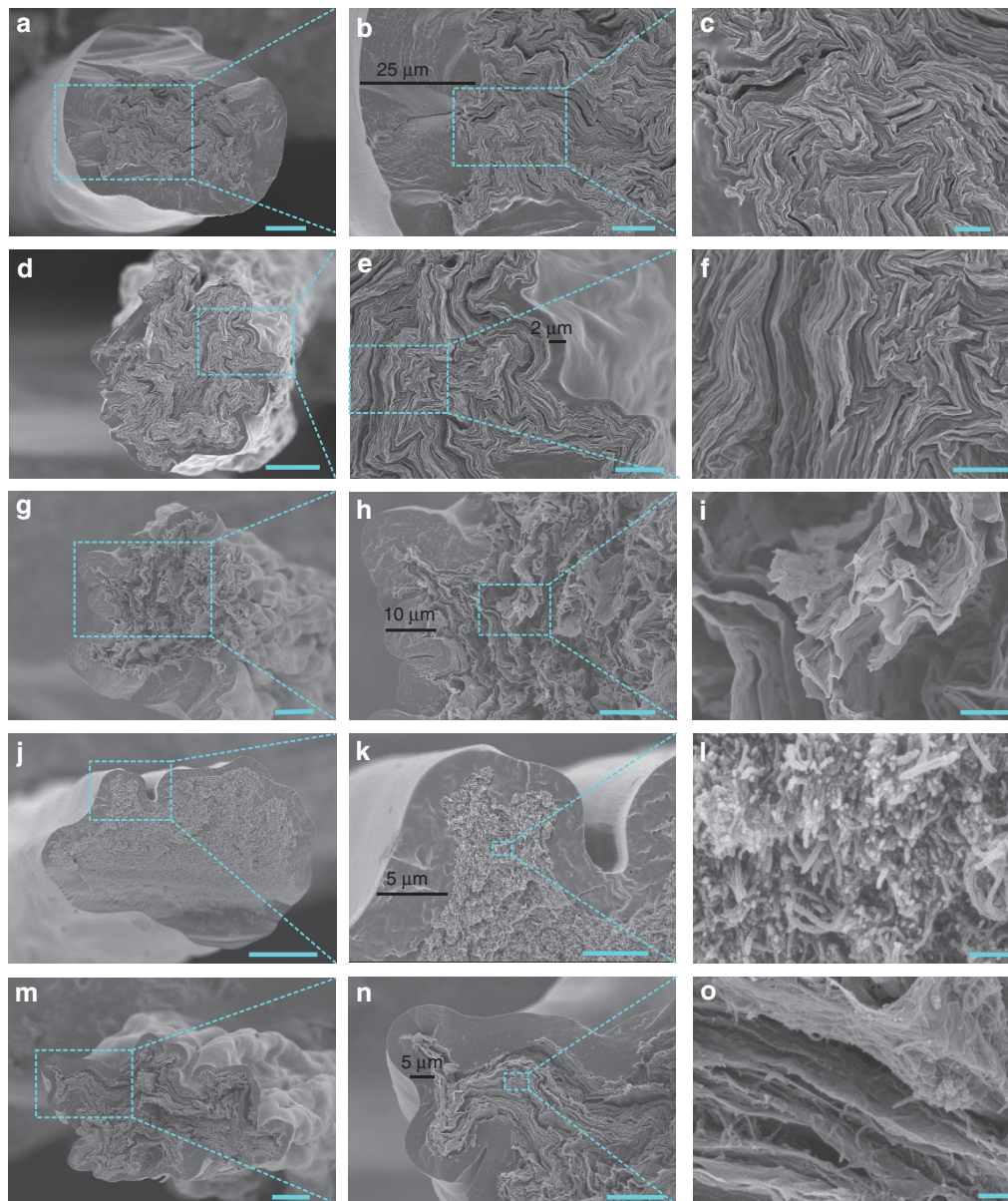


Figure 2 | SEM images of coaxial fibres. (a–c) GO@CMC spun with GO of 20 mg ml^{-1} and CMC of 12 mg ml^{-1} . (d–f) GO@CMC spun with GO of 20 mg ml^{-1} and CMC of 4 mg ml^{-1} . (g–i) RGO@CMC spun with GO of 20 mg ml^{-1} and CMC of 8 mg ml^{-1} . (j–l) CNT@CMC spun with CNT of 10 mg ml^{-1} and CMC of 8 mg ml^{-1} . (m–o) RGO + CNT@CMC spun with GO and CNT mixture (w/w, 1/1) of 20 mg ml^{-1} and CMC of 8 mg ml^{-1} . Scale bars, $20 \mu\text{m}$ (a,d,g,j,m), $10 \mu\text{m}$ (b,h,n), $5 \mu\text{m}$ (e,k), $2 \mu\text{m}$ (c,f,i) and $0.2 \mu\text{m}$ (l,o).

Coaxial fibres assembled two-ply YSCs. Given the unique attributes of the core-sheath coaxial fibres, we directly used them as safe electrodes for making two-ply YSCs. The YSCs were prepared by tightly intertwining two coaxial fibres followed by coating a layer of H_3PO_4 -PVA gel electrolyte as ion source (Fig. 3a,b)⁸. The as-prepared YSCs are very safe, and short circuit never happened in the assembly and working process of YSCs because of the protection of the CMC sheath. The cross-sectional view of the YSC shows that the coaxial structure of the fibre electrodes is well reserved (Fig. 3a). The H_3PO_4 -PVA gel electrolyte was coated on the coaxial fibre electrodes tightly and penetrated into the gap between them, which is important for the high capacitance performance of YSCs. The side view of the YSC indicates the uniform coating of PVA electrolyte and the clearly intertwined morphology of the two fibres (Fig. 3b). Significantly, the two-ply YSC is flexible enough to make a

compact knot and the two fibre electrodes are observed along the YSC (Fig. 3c).

We first assembled two kinds of two-ply YSCs with neat graphene (RGO@CMC) and neat CNT (CNT@CMC) coaxial fibres, respectively, to testify the feasibility of our strategy. The electrochemical properties of the as-prepared YSCs were characterized by cyclic voltammetry (CV), galvanostatic charge-discharge (GCD) measurements. For the YSCs intertwined with RGO@CMC fibres, the CV curves show a nearly rectangular shape and a rapid current response to voltage reversal at each end potential (Fig. 3d), which illustrates the good electrochemical performance of the YSCs. Figure 3g shows the GCD behaviour of RGO@CMC YSCs between 0 and 0.8 V at different current densities (0.1 – 1.0 mA cm^{-2}). The GCD curves are close to triangular shape, confirming the formation of an efficient electric double layers and good charge propagation across the two fibre

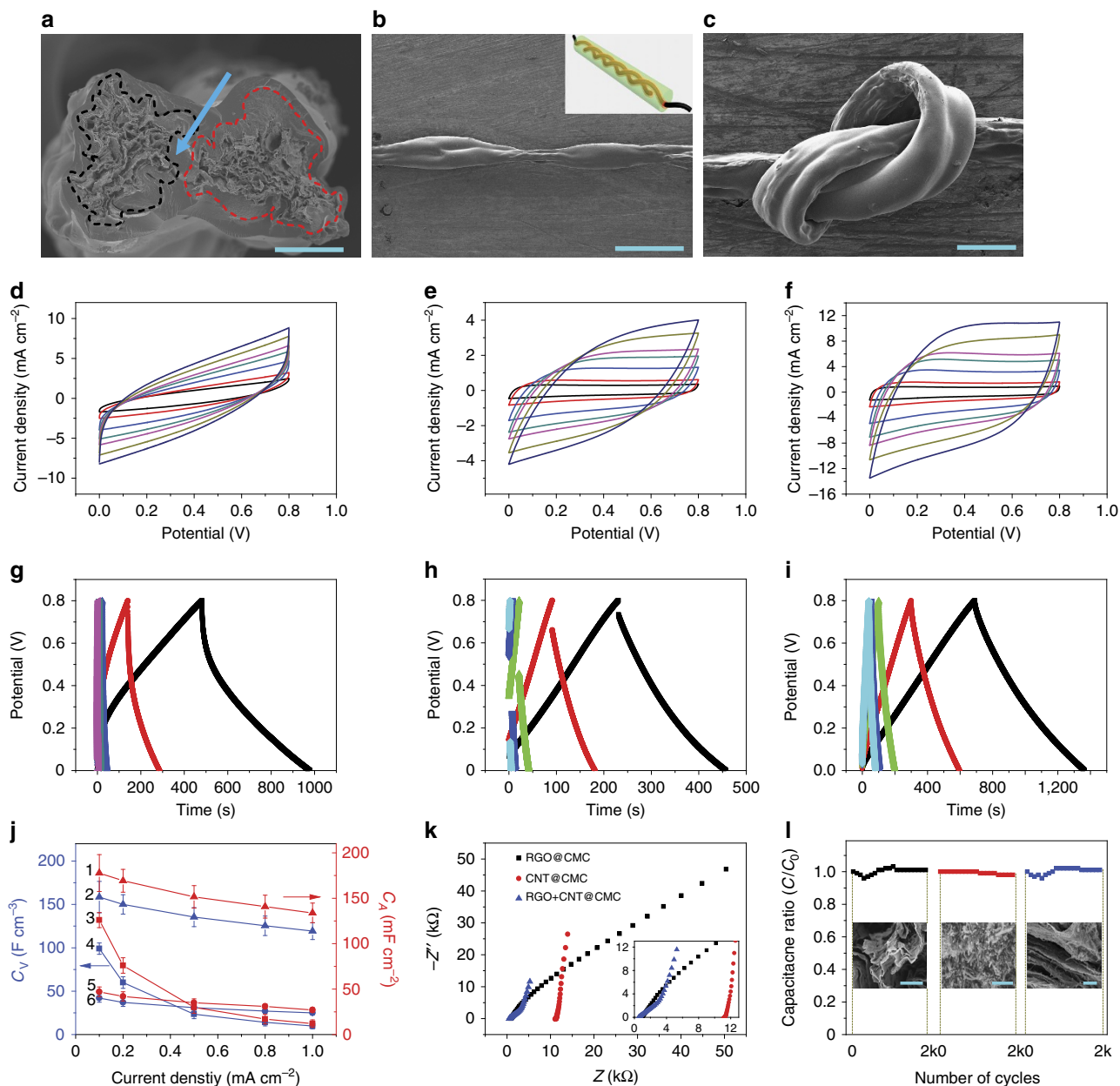


Figure 3 | Two-ply YSCs and their electrochemical properties. SEM images of cross-sectional (**a**) and side (**b**) view of a two-ply YSC. The arrow area in **a** is PVA/H₃PO₄ electrolyte and inset of **b** shows the schematic illustration of YSC. (**c**) SEM image of a two-ply YSC knot. CV curves of RGO@CMC (**d**), CNT@CMC (**e**) and RGO + CNT@CMC (**f**), scan rates increased from 10 to 20, 50, 80, 100, 150 and 200 mV s⁻¹. GCD curves of RGO@CMC (**g**), CNT@CMC (**h**) and RGO + CNT@CMC (**i**), current density increased from 0.1 to 0.2, 0.5, 0.8 and 1 mA cm⁻². (**j**) Dependence of C_A and C_V on the charge/discharge current density for RGO@CMC (3, 4), CNT@CMC (5, 6) and RGO + CNT@CMC (1, 2) YSCs. We selected five cross-sections and used the average value as the cross-sectional areas to determine the error bars. (**k**) Nyquist plots of RGO@CMC, CNT@CMC and RGO + CNT@CMC YSCs. (**l**) Normalized capacitance (C/C_0 , where C_0 is the initial capacitance) versus cycle number for RGO@CMC (left), CNT@CMC (middle) and RGO + CNT@CMC (right) YSCs. Scale bars, 50 μ m (**a**), 500 μ m (**b**), 200 μ m (**c**), 3 μ m for left and 0.3 μ m for middle and right (**l**).

electrodes²⁹. Gram capacitance does not provide a suitable basis for comparison in YSCs³⁰. Instead, for the convenience of comparing with the previous results, areal capacitance (C_A), length capacitance (C_L) and volume capacitance (C_V) are commonly utilized to evaluate the charge-storage capacity of YSCs (Table 1; note: the capacitances denote those of single electrodes). Calculated from the GCD curves (Fig. 3g), C_{AS} of RGO@CMC YSCs are extremely high with capacitance of 127 mF cm⁻² (114 F cm⁻³ for C_V , 3.8 mF cm⁻¹ for C_L) at the current density of 0.1 mA cm⁻². Such a capacitance is two orders of magnitude higher than those of previous graphene YSCs³.

For CNT@CMC YSCs, the CV curves also show the desired rectangular dependence of current density on applied potential because of fast ion transportation (Fig. 3e). The GCD curves exhibit a relatively high potential drop (Fig. 3h), which is likely stemmed from the larger resistance of carboxylic CNTs. Nevertheless, CNT@CMC YSCs still showed a C_A 47 mF cm⁻² (C_V 42 F cm⁻³, C_L 1.4 mF cm⁻¹) at the current density of 0.1 mA cm⁻², around 20 times higher than that of previous neat CNT YSCs⁵.

The two cases of RGO@CMC and CNT@CMC YSCs efficiently demonstrate that the polyelectrolyte sheath not only endows the fibre electrodes' safety (free of short circuit when directly

Table 1 | Comparison of our YSCs with the reported YSCs in terms of C and E.

Ref.	Electrode materials	C			E	
		C_A (mF cm ⁻²)	C_V (F cm ⁻³)	C_L (mF cm ⁻¹)	E_A (μWh cm ⁻²)	E_V (mWh cm ⁻³)
This study	RGO + CNT	177	158	5.3	3.84	3.5
1	Pen ink	26.4		1.008	2.7	
3	Graphene	1.7			0.17	
5	PANI/CNT	38				
7	CNT/OMC	39.7		1.91	1.77	
8	CNT/MnO ₂	3.01		0.015		1.73
10	PEDOT/CNT	73	179	0.47		1.4
11	ZnO nanowires/MnO ₂	2.4		0.04	0.027	
31	CNT and Ti fibres	0.6		0.024	0.15	
32	Graphene	0.726		0.01		
33	ZnO nanowires/graphene	2		0.025		
38	PANI/stainless steel	41			0.95	
39	Carbon/MnO ₂		2.5			0.22

CNT, carbon nanotube; OMC, ordered mesoporous carbon; PANI, polyaniline; PEDOT, poly(3,4-ethylenedioxythiophene); YSC, Yarn supercapacitor.

entangled together) but also remarkably improves the performance of YSCs. Therefore, the creation of coaxial fibre supercapacitors gives brand-new insight for the design and optimization of YSCs and other electronic devices.

Furthermore, the capacitance of supercapacitors at high charge–discharge current density is also crucial for their practical application as energy-storage devices. We also tested the charge–discharge performance at different current densities for the coaxial fibre YSCs. As shown in Fig. 3j, the C_{AS} of RGO@CMC YSCs decreased quickly from 127 to 30 mF cm⁻² as the current density increased from 0.1 to 0.5 mA cm⁻², and then decreased gradually to 10 mF cm⁻² at the current density of 1.0 mA cm⁻². Even so, the C_A values are still quite high at the high current densities as compared with the previous neat graphene fibre-based YSCs (1.2 mF cm⁻² at current of 2 μA). The considerable difference of capacitance between low and high current densities partly counteracts the high potential of RGO@CMC YSCs. By contrast, the CNT@CMC YSCs showed very stable C_A and still kept 57% of capacitance as the current density increased from 0.1 to 1 mA cm⁻² (Fig. 3j), likely because of the smooth ion access in the porous structures of CNTs.

A question is then raised: is it possible to access ideal YSCs with both features of large C_A and high rate capability by the synergistic assembly of graphene and CNTs?

Ultra-high performance of RGO + CNT@CMC YSCs. To exploit such a kind of desired YSCs, we also fabricated YSCs with the electrodes of RGO + CNT@CMC coaxial fibres. The fibres contained the electrically conductive core assembled homogeneously by RGO and CNTs (Fig. 2o). Interestingly, the RGO + CNT@CMC YSCs showed much larger area circled by rectangular shaped CV curves (Fig. 3f) and more regular triangular shaped GCD curves (Fig. 3i). The discharge time of RGO + CNT@CMC YSCs reached 700 s at the current density of 0.1 mA cm⁻², almost equal to the sum of those of RGO@CMC (497 s) and CNT@CMC YSCs (174 s), indicating the prominent enhancement of stored charges (or capacitance) for the synergistically assembled electrodes of RGO + CNTs. Hence, the RGO + CNT@CMC YSCs demonstrated much better electrochemical performance with C_A of 177 mF cm⁻² (C_V 158 F cm⁻³ and C_L 5.3 mF cm⁻¹) at the current density of 0.1 mA cm⁻². This C_A value is obviously higher than either C_A of CNT@CMC YSCs or that of RGO@CMC YSCs, approximating the total capacitance of the two YSCs (127 + 47 mF cm⁻²) under

the same testing condition. This result suggests that a single device of RGO + CNT@CMC YSC corresponds to the parallel connection of one RGO@CMC YSC and one CNT@CMC YSC. The capacitance of RGO + CNT@CMC YSC can be further highly improved to 269 mF cm⁻² (C_V 239 F cm⁻³ and C_L 8.0 mF cm⁻¹) by using liquid electrolyte of 1 M H₂SO₄ aqueous solution (Supplementary Fig. 10). More significantly, the RGO + CNT@CMC YSCs also inherited the high rate capability merit of CNT@CMC YSCs and exhibited high retention (75%) of capacitance at a high current density of 1 mA cm⁻² (Fig. 3j). Accordingly, ideal YSCs with both natures of ultra-high capacitance and excellent rate capability are achieved by the combination of coaxial wet-spinning assembly approach and the synergistic effect of graphene and CNTs.

The superior electrochemical performance of RGO + CNT@CMC YSCs can be also explained by the smaller intrinsic internal resistance (R) measured from corresponding electrochemical impedance spectroscopy (Fig. 3k). RGO + CNT@CMC YSCs had a smaller R (0.55 KΩ) than RGO@CMC (0.87 KΩ) and CNT@CMC YSCs (11.22 KΩ) on the real axis at high frequency. Moreover, RGO + CNT@CMC YSCs showed a relatively short 45° Warburg region at the middle frequency, and a more vertical line at low frequency, indicating much better electrochemical performance³¹.

For comparison, we summarized the C_A , C_V and C_L values of our and the previously reported YSCs in Table 1. Generally, for our YSCs with solid electrolyte of H₃PO₄/PVA, the C_A (177 mF cm⁻²) based on the coaxial fibres is higher than those of the ever best YSCs (73 and 86.8 mF cm⁻²) by about 100% and is one to three order of magnitude higher than those of common YSCs (0.4–38 mF cm⁻²) even containing the additional electrically active materials such as metal oxides and conductive polymers^{32,33}. The C_L of our YSCs (5.3 mF cm⁻¹) is comparable to the ever highest value (6.3 mF cm⁻¹) and is one to three order of magnitude higher than those of other YSCs (0.0114–0.504 mF cm⁻¹)^{1,33}. Besides, C_V of our YSCs is 158 F cm⁻³, which is comparable to that of CNT/PEDOT YSCs (179 F cm⁻³)¹⁰. For our YSCs with liquid electrolyte of 1 M H₂SO₄ aqueous solution, C_V is improved to 239 F cm⁻³, which is obviously higher than that of CNT/PEDOT YSCs with liquid electrolyte (~167 F cm⁻³).

In addition, all these three kinds of YSCs showed almost no decay of capacitance within 2,000 times of charge–discharge cycles (Fig. 3l) over the range from 0 to 0.8 V at a current density of 1 mA cm⁻². Leakage current was also measured by charging YSCs to 0.8 V and keeping them for 2 h (Supplementary Fig. 11).

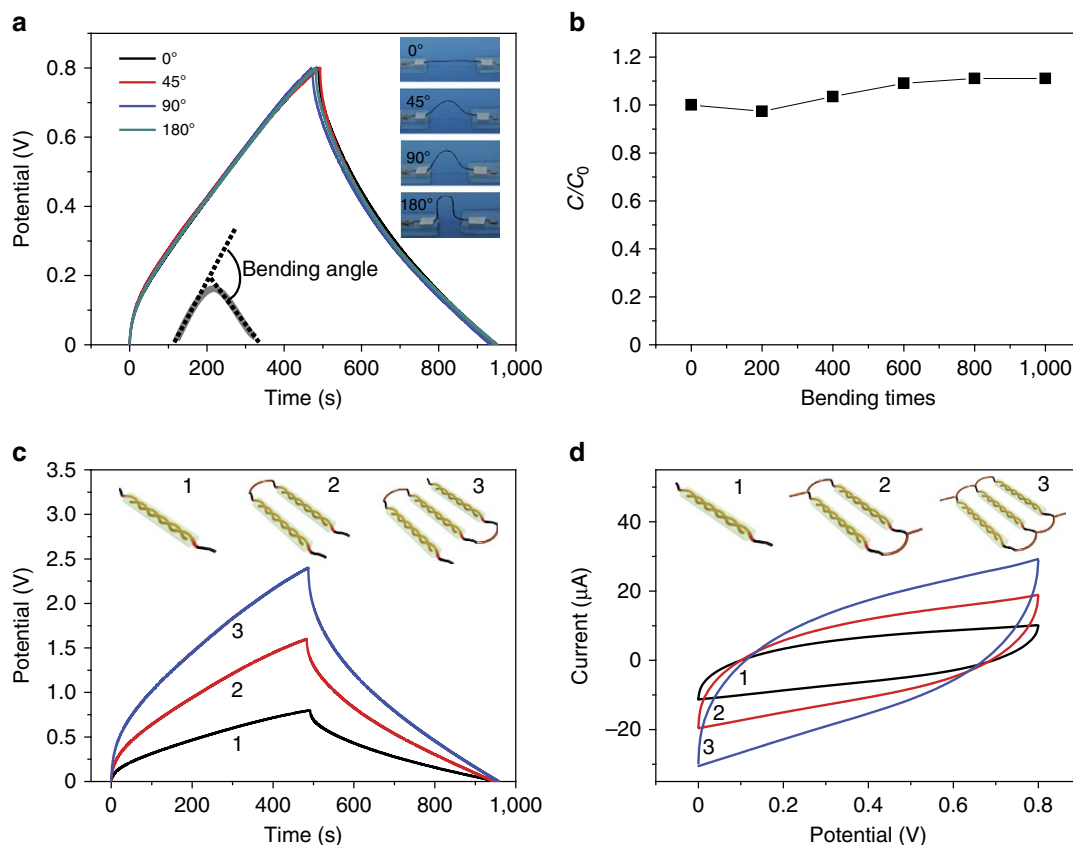


Figure 4 | The capacitance performance of YSCs under bending and series/parallel connections. (a) GCD curves of two-ply, all-solid-state, free-standing YSCs bended with different angles at the current density of 0.1 mA cm^{-2} , and the insets are the digital photos of YSCs with different bending angles. (b) Capacitance ratio (C/C_0 , where C_0 is the initial capacitance) versus bending times for YSCs with bending angles of 180° . (c) GCD curves of single, two and three YSCs connected in series, and the insets depict the cartoon of the YSCs connected in series. (d) CV curves of single, two and three YSCs connected in parallel, and the insets show the corresponding schematics (scan rates, 10 mV s^{-1}).

The current quickly stabilizes at $0.8 \mu\text{A}$, which is essentially the leakage current through the device, indicating a small leakage current and high stability of our YSCs. Such excellent stability is competitive in the practical applications of YSCs.

Flexibility and connections of two-ply YSCs. Unlike the liquid electrolyte with the risk of electrolyte leakage, our all-solid-state flexible YSCs are highly flexional and were even tied into a knot (Fig. 3c). We tested the GCD curves of the two-ply YSCs under different bending angles (for example, 45° , 90° and 180°), as shown in Fig. 4a. Almost no change for the charge–discharge curves was observed during the bending, proving that the inner structures of YSCs maintained well even at a sharp bending state. The coaxial fibre YSCs are flexible and robust enough to tolerate the long-term and repeated bending, and the capacitance only dropped 2% at 200 times of bending and rose persistently up to 111% at 1,000 times of bending (Fig. 4b).

Owing to the flexibility of our two-ply YSCs, we further made their serial and parallel connections to control over the operating voltage and current. With almost the same discharge time, the operating voltage can be elevated from 0.8 V for single YSC to 1.6 and 2.4 V by connecting two and three YSCs in series, respectively (Fig. 4c). The output currents of two and three YSCs connected in parallel are doubled and tripled, respectively, with a same potential window of 0–0.8 V (Fig. 4d).

Coaxial fibre-woven cloth supercapacitors. The integration of high flexibility and scalable fabrication of our coaxial fibres

promises highly potential application in garment devices, bio-medical and antimicrobial textiles, and personal electronics³⁴. Figure 5a shows a co-woven cloth using multiple cotton yarns and two intact coaxial fibres. The fibres are flexible enough to shuttle back and forth without fracture, as demonstrated by the optical microscopy image of the co-woven cloth (Fig. 5b). For the first time, we used two individual 40-cm-long coaxial RGO + CNT@CMC fibres as anode and cathode to interweave a cloth supercapacitor (Fig. 5c,d). Previously, multiple short CNT/PANI fibres were woven into a piece of cloth, but no electrochemical property was evaluated⁵; one two-ply supercapacitor (5 cm long) was straightly drawn across a cotton grove, but no interweaving of two electrodes was demonstrated¹⁰. In other words, cloth supercapacitors interwoven from individual intact fibre electrodes have never been reported. In our case, short circuit of the fibre electrodes was avoided at the crossing of the cloth because of the unique coaxial insulated polyelectrolyte-wrapped structure. Our cloth supercapacitor showed a capacitance of 28 mF at the current of $10 \mu\text{A}$ (Fig. 5e), higher than 25 mF of commercial supercapacitors³⁵. The corresponding GCD curves were unchanged under the bending angle of 180° along the three directions shown in the inset of Fig. 5e, revealing the excellent bendability of our cloth supercapacitors woven from coaxial fibres.

Discussion

As shown above, our two-ply YSCs possess the various merits of ultra-high capacitance, good rate capability, excellent cycling

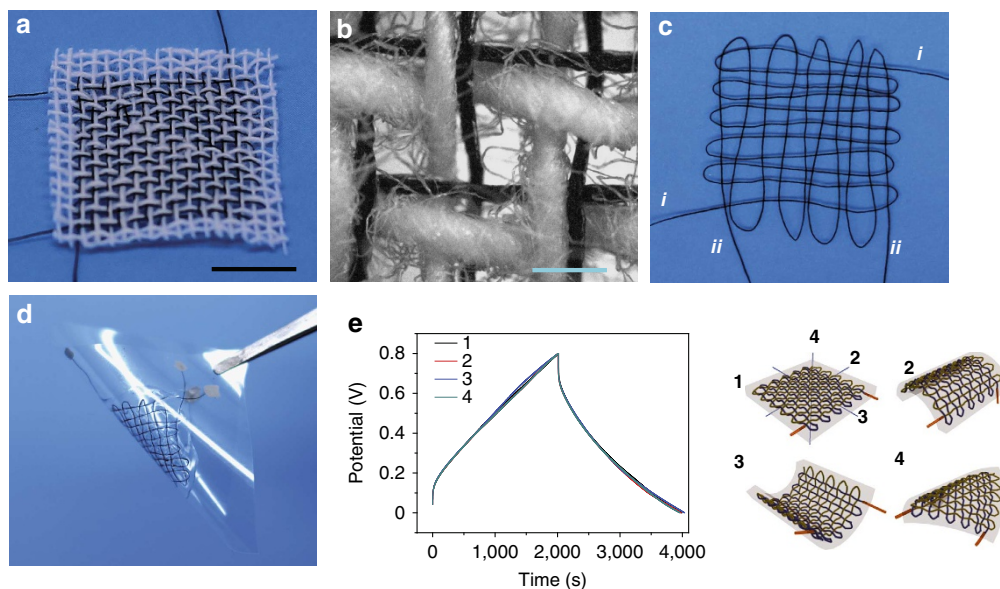


Figure 5 | Supercapacitor based on the cloth woven by coaxial fibres. (a) Two intact coaxial fibres woven with cotton fibres. (b) Optical macroscopic image of a. (c) Cloth woven by two individual coaxial fibres. (d) Supercapacitor device based on the cloth fabricated by two coaxial fibres (denoted as *i* and *ii*, respectively). (e) GCD curves of the cloth supercapacitor (1 represents initial cloth supercapacitor without bending, and 2, 3, 4 show cloth supercapacitor with bending angles of 180° along three directions). Scale bars, 1 cm (a) and 200 μm (b).

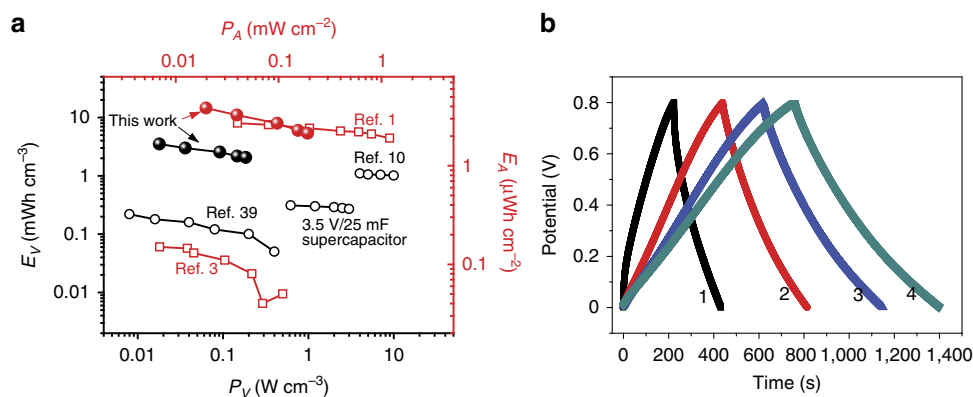


Figure 6 | Volumetric and areal energy versus average power densities and the shell thickness effect for RGO + CNT@CMC YSCs. (a) Ragone plots compared with the selected previous fibre-shaped YSCs with solid electrolyte. (b) GCD curves at the current density of 0.1 mA cm⁻² for RGO + CNT@CMC fibres with CMC shell thickness of 0 μm (1), 2 μm (2), 10 μm (3) and 25 μm (4).

stability, high flexibility and knittability, and fine modulability of connection. Besides, E and P of supercapacitors are also quite important parameters for their real applications^{34,36}. We then draw the profile of P versus E , so-called Ragone plot³⁷, derived from GCD curves at various current densities from 0.1 to 1 mA cm⁻² for the RGO + CNT@CMC YSCs (Fig. 6a). As a result, the YSC using solid electrolyte shows areal energy density (E_A) of 3.84 μWh cm⁻² and volumetric energy density (E_V) of 3.5 mWh cm⁻³, while the areal power density (P_A) and volumetric power density (P_V) is 0.02 mW cm⁻² and 0.018 W cm⁻³ at the current density of 0.1 mA cm⁻², respectively.

Notably, as far as we know, our E_A value is the highest energy density for all of reported YSCs (Table 1). As a quantitative comparison, it corresponds to 142 times of YSC based on ZnO nanowires/MnO₂ (0.027 μWh cm⁻²)¹¹, 26 times of YSC based on CNT and Ti fibres (0.15 μWh cm⁻²)³¹, 22 times of YSC based on

core-sheath graphene fibres (0.17 μWh cm⁻²)³, 4 times of YSC based on PANI/stainless steel (0.95 μWh cm⁻²)³⁸, 2.17 times of YSC based on CNT/ordered mesoporous carbon (1.77 μWh cm⁻²)⁷ and 1.42 times of YSC based on pen ink (2.7 μWh cm⁻²)¹. Alternatively, E_V of RGO + CNT@CMC YSCs is 3.5 mWh cm⁻³, around 16 times of YSC based on carbon/MnO₂ (0.22 mWh cm⁻³)³⁹ and two times of YSC based on CNT/MnO₂ fibres (1.73 mWh cm⁻³)⁸.

The excellent electrochemical performance of our YSCs is likely resulted from three effects. First, during coagulation and drying process for the coaxial wet-spinning technology, the shrinkage speed of the outer CMC layer is faster than that of the inner GO or CNTs core, making CMC sheath wrap the graphene or CNTs tightly (Supplementary Fig. 6). This is crucial for better ion transport at the interface between electrolyte and the electrodes. Second, this coaxial wet-spinning process renders the pore structures of inner GO or CNTs core more elaborate

because of the uniform shrinkage force of the CMC sheath. The thicker the CMC sheath is, the stronger the shrinkage force would be generated during the drying process. Therefore, the C_A of RGO + CNT@CMC YSCs increased from 35 to 103, 145 and 177 mF cm^{-2} with increasing the thickness of CMC sheath from 0 (Supplementary Fig. 12) to 2, 10 and 25 μm (Supplementary Fig. 13). To further demonstrate the merits of the coaxial wet-spinning assembly strategy, we assembled two more YSCs in control experiments using naked RGO + CNT fibres fabricated by conventional wet-spinning method¹² and RGO + CNT fibres post-coated with CMC as electrodes, respectively. After post-coating a CMC layer on the surface of naked RGO + CNT fibres, the capacitance (39 mF cm^{-2}) is almost same as that of the initial naked RGO + CNT fibre without CMC coating (35 mF cm^{-2}) but much smaller than that of coaxial wet-spun fibres (103 mF cm^{-2}) at the current density of 0.1 mA cm^{-2} . The CV curves of CMC post-coating YSC and naked fibre YSC are almost overlapped, whereas much smaller than those of coaxial wet-spun fibre YSC (Supplementary Fig. 14e). These control experiments clearly demonstrated that CMC has no pseudocapacitance effect and the dramatic improvement of electrochemical performance for coaxial wet-spun fibre-based YSCs is mainly ascribed to the coaxial wet-spinning assembly process. Meanwhile, the rate capability is also excellent for the coaxial wet-spun fibre YSCs. For RGO + CNT@CMC YSCs with CMC thickness of 2, 10 and 25 μm , the capacitances are retained by 84%, 77% and 75%, respectively, when the current density is increased from 0.1 to 1 mA cm^{-2} (Supplementary Fig. 13). The slightly different rate capability is likely caused by the increased thickness of CMC, which might lead to a longer distance between the two fibre electrodes. As a result, ion transport is affected to some extent at high current densities. Finally, the synergistic effect that arose from the hierarchical structures of CNT-coated graphene makes the C and E of RGO + CNT@CMC YSC superior to either RGO@CMC or RGO + CNT@CMC YSC. Therefore, the combination of the coaxial wet-spinning process and the hierarchical structures of CNT-coated graphene mainly contributes to the high performance of RGO + CNT@CMC YSCs.

In conclusion, we proposed and demonstrated for the first time a coaxial wet-spinning assembly strategy to prepare core-sheath fibres of polymer-wrapped carbon nanomaterials. The protocol is simple, industrially viable and general for both nanoparticles of graphene and CNTs that cannot be wet-spun continuously by previous approaches. The as-made coaxial fibres are flexible and robust enough to be intertwined, knotted and woven. Owing to the coating of electrically insulative polyelectrolyte, the coaxial fibres were used directly to assembly two-ply intertwined safe YSCs. The resultant RGO + CNT@CMC YSCs showed ultra-high capacitance, the record energy density and excellent cycle stability under bending. A highly bendable cloth supercapacitor was woven from two 40-cm-long coaxial fibres, promising the application of our YSCs in garment devices, intelligent micro-sensors and other wearable electronics. The electrically active metal oxides (for example, MnO_2 , NiO and RuO_2) and conductive polymers can widely be integrated into the coaxial fibres to further improve the electrochemical performance of YSCs⁴⁰, offering a wide approach to the next generation of smart, safe and flexible devices.

Methods

Preparation of coaxial fibres by coaxial wet-spinning. GO and CNT dispersions were prepared according to the previous reports^{41–44}. For preparing RGO@CMC, GO dispersion was concentrated to $\sim 20 \text{ mg ml}^{-1}$ and transferred to an injection syringe connected with an inner core of spinneret. CMC (Aladdin) dissolved in water with concentration of $\sim 8 \text{ mg ml}^{-1}$ was transferred to the outer channel of spinneret. The typical extruded velocities of inner and outer layers were set at 10 and 40 $\mu\text{l min}^{-1}$, respectively. The coagulating bath was ethanol/water (5:1 v/v)

solution with 5 wt% CaCl_2 . After coagulation for 30 min, the fibres were immersed in hydriodic acid ethanol/water (5:1 v/v) solution for 1 h at 95 °C for reduction followed by ethanol washing and drying in air, affording RGO@CMC coaxial fibres. The CNT@CMC coaxial fibres were prepared with the same procedure by replacing GO with CNT aqueous dispersions. Likewise, for spinning RGO + CNT@CMC coaxial fibres, GO and CNT dispersions were first mixed with weight ratio of 1/1 by magnetic stirring for 2 h and then were used as the inner spinning dope.

Preparation of PVA solid electrolyte. Water (10 ml) and phosphoric acid (10 ml) were mixed by magnetic stirring for 30 min in a 250-ml glass bottle. PVA (10 g, Mw 89,000–98,000) dissolved in 90 ml water at 90 °C was added in the above solution and was kept stirring for 1 h.

Preparation of free-standing all-solid-state fibre supercapacitors. Two coaxial fibres were twisted together to form two-ply supercapacitor electrodes. They were then coated with PVA electrolyte by dip-coating method and solidification at 40 °C.

Apparatus for characterizations. Atomic force microscopy images were taken in the tapping mode by carrying out on a NSK SPI3800. SEM images were taken on a Hitachi S4800 field-emission SEM system. The core-sheath fibre was cut into slices by microtome and observed by TEM (FEI-PHILLIPS CM 200 electron microscope). Polarized-light optical microscopy observations were performed with a Nikon E600POL. CV, electrochemical impedance spectroscopy and GCD measurements were performed using an electrochemical workstation (CHI660e, CH Instruments Inc.). The tensile stress-strain tests were performed on a Micro-computer Control Electronic Universal Testing Machine made by REGER in China (RGWT-4000-20).

Calculation of the electrochemical capacitance for two-ply electrode supercapacitors. The two-ply YSC is a symmetric two-electrode solid-state supercapacitor. The areal capacitance (C_A) was derived from the equation: $C_A = I \times t \times U^{-1} \times S^{-1}$, where I stands for discharge-discharge current, t is the discharge time, U represents the potential window and S is the surface area of single yarn in the overlapping portion, equal to the circumference of the cross-section multiplied by the length (L) of overlapped portion of fibre electrodes⁵. Circumference is measured by using a soft rope walked along the cross profile of the SEM images of the fibres. C_V was derived from the equation: $C_V = C_A \times S \times V^{-1}$. V is the volume of the fibre electrode, which is equal to the cross-sectional area multiplied by the length of overlapped portion of fibre electrodes. Cross-sectional areas are measured through Photoshop (image-processing software) by comparing the pixel with that of an internal reference. The length capacitance C_L was derived from the equation: $C_L = C_A \times S \times L^{-1}$. The areal energy density (E) and areal power density (P) of the YSCs can be obtained from $E_A = 0.125 \times C_A \times U^2$ and $P_A = E_A \times t^{-1}$. The volumetric energy density (E) and volumetric power density (P) of the YSCs can be obtained from $E_V = 0.125 \times C_V \times U^2$ and $P_V = E_V \times t^{-1}$.

References

- Fu, Y. *et al.* Fibre supercapacitors utilizing pen ink for flexible/wearable energy storage. *Adv. Mater.* **24**, 5713–5718 (2012).
- Wang, G., Zhang, L. & Zhang, J. A review of electrode materials for electrochemical supercapacitors. *Chem. Soc. Rev.* **41**, 797–828 (2012).
- Meng, Y. *et al.* All-graphene core-sheath microfibres for all-solid-state, stretchable fibriform supercapacitors and wearable electronic textiles. *Adv. Mater.* **25**, 2326–2331 (2013).
- Le, V. T. *et al.* Coaxial fibre supercapacitor using all-carbon material electrodes. *ACS Nano* **7**, 5940–5947 (2013).
- Wang, K., Meng, Q., Zhang, Y., Wei, Z. & Miao, M. High-performance two-ply yarn supercapacitors based on carbon nanotubes and polyaniline nanowire arrays. *Adv. Mater.* **25**, 1494–1498 (2013).
- Huang, T. *et al.* Flexible, high performance wet-spun graphene fiber supercapacitors. *RSC Adv.* **3**, 23957–23962 (2013).
- Ren, J. *et al.* Flexible and weavable capacitor wire based on a carbon nanocomposite fiber. *Adv. Mater.* **25**, 5695–5670 (2013).
- Ren, J. *et al.* Twisting carbon nanotube fibres for both wire-shaped micro-supercapacitor and micro-battery. *Adv. Mater.* **25**, 1155–1159 (2013).
- Tao, J. *et al.* Solid-State High performance flexible supercapacitors based on polypyrrole-MnO₂-carbon fibre hybrid structure. *Sci. Rep.* **3**, 2286 (2013).
- Lee, J. A. *et al.* Ultrafast charge and discharge bisrolled yarn supercapacitors for textiles and microdevices. *Nat. Commun.* **4**, 1970 (2013).
- Bae, J. *et al.* Fibre supercapacitors made of nanowire-fibre hybrid structures for wearable/flexible energy storage. *Angew. Chem. Int. Ed.* **50**, 1683–1687 (2011).
- Xu, Z. & Gao, C. Graphene chiral liquid crystals and macroscopic assembled fibres. *Nat. Commun.* **2**, 571 (2011).

13. Xu, Z., Sun, H., Zhao, X. & Gao, C. Ultrastrong fiber assembled from giant graphene oxide sheets. *Adv. Mater.* **25**, 188–193 (2013).
14. Pei, S., Zhao, J., Du, J., Ren, W. & Cheng, H.-M. Direct reduction of graphene oxide films into highly conductive and flexible graphene films by hydrohalic acids. *Carbon*. **48**, 4466–4474 (2010).
15. Kou, L. & Gao, C. Bioinspired design and macroscopic assembly of poly(vinyl alcohol)-coated graphene into kilometers-long fiber. *Nanoscale* **5**, 4370–4378 (2013).
16. Jalili, R. *et al.* Scalable one-step wet-spinning of graphene fiber and yarns from liquid crystalline dispersions of graphene oxide: towards multifunctional textiles. *Adv. Funct. Mater.* **23**, 5345–5354 (2013).
17. Cong, H.-P., Ren, X.-C., Wang, P. & Yu, S.-H. Wet-spinning assembly of continuous, neat, and macroscopic graphene fibers. *Sci. Rep.* **2**, 613 (2012).
18. Chen, L. *et al.* Toward high performance graphene fibers. *Nanoscale* **5**, 5809–5815 (2013).
19. Xu, Z., Liu, Z., Sun, H. & Gao, C. Highly electrically conductive Ag-doped graphene fibers as stretchable conductors. *Adv. Mater.* **25**, 3249–3253 (2013).
20. Dong, Z. *et al.* Facile fabrication of light, flexible and multifunctional graphene fibers. *Adv. Mater.* **24**, 1856–1861 (2012).
21. Xu, Z., Zhang, Y., Li, P. & Gao, C. Strong, conductive, lightweight, neat graphene aerogel fibers with aligned pores. *ACS Nano* **6**, 7103–7113 (2012).
22. Zhao, Y. *et al.* Large-scale spinning assembly of neat, morphology-defined, graphene-based hollow fibres. *ACS Nano* **7**, 2406–2412 (2013).
23. Hu, X., Xu, Z. & Gao, C. Multifunctional, supramolecular, continuous artificial nacre fibres. *Sci. Rep.* **2**, 767 (2012).
24. Liu, Z., Xu, Z., Hu, X. & Gao, C. Lyotropic liquid crystal of polyacrylonitrile-grafted graphene oxide and its assembled continuous strong nacre-mimetic fibres. *Macromolecules* **46**, 6931–6941 (2013).
25. Sun, Z., Zussman, E., Yarin, A. L., Wendorff, J. H. & Greiner, A. Compound core-sheath polymer nanofibres by co-electrospinning. *Adv. Mater.* **15**, 1929–1932 (2003).
26. Kou, L. & Gao, C. Making silica nanoparticle-covered graphene oxide nanohybrids as general building blocks for large-area superhydrophilic coatings. *Nanoscale* **3**, 519–528 (2011).
27. Kou, L., He, H. & Gao, C. Click chemistry approach to functionalize two-dimensional macromolecules of graphene oxide nanosheets. *Nano Micro. Lett.* **2**, 177–183 (2010).
28. Vigolo, B. *et al.* Macroscopic fibres and ribbons of oriented carbon nanotubes. *Science* **290**, 1331–1334 (2000).
29. Yoo, J. J. *et al.* Ultrathin planar graphene supercapacitors. *Nano Lett.* **11**, 1423–1427 (2011).
30. Gogotsi, Y. & Simon, P. True performance metrics in electrochemical energy storage. *Science* **334**, 917–918 (2011).
31. Chen, T. *et al.* An integrated ‘energy wire’ for both photoelectric conversion and energy storage. *Angew. Chem. Int. Ed.* **51**, 11977–11980 (2012).
32. Li, Y., Sheng, K., Yuan, W. & Shi, G. A high-performance flexible fibre-shaped electrochemical capacitor based on electrochemically reduced graphene oxide. *Chem. Commun.* **49**, 291–293 (2013).
33. Bae, J. *et al.* Single-fiber-based hybridization of energy converters and storage units using graphene as electrodes. *Adv. Mater.* **23**, 3446–3449 (2011).
34. Jost, K. *et al.* Carbon coated textiles for flexible energy storage. *Energ. Environ. Sci.* **4**, 5060–5067 (2011).
35. Pech, D. *et al.* Ultrahigh-power micrometre-sized supercapacitors based on onion-like carbon. *Nat. Nanotech.* **5**, 651–654 (2010).
36. Zhai, Y. *et al.* Carbon materials for chemical capacitive energy storage. *Adv. Mater.* **23**, 4828–4850 (2011).
37. Service, R. F. New ‘supercapacitor’ promises to pack more electrical punch. *Science* **313**, 902 (2006).
38. Fu, Y. *et al.* Integrated power fibre for energy conversion and storage. *Energ. Environ. Sci.* **6**, 805–812 (2013).
39. Xiao, X. *et al.* Fibre-based all-solid-state flexible supercapacitors for self-powered systems. *ACS Nano* **6**, 9200–9206 (2012).
40. Simon, P. & Gogotsi, Y. Materials for electrochemical capacitors. *Nat. Mater.* **7**, 845–854 (2008).
41. He, H. & Gao, C. General approach to individually dispersed, highly soluble, and conductive graphene nanosheets functionalized by nitrene chemistry. *Chem. Mater.* **22**, 5054–5064 (2010).
42. Kan, L., Xu, Z. & Gao, C. General avenue to individually dispersed graphene oxide-based two-dimensional molecular brushes by free radical polymerization. *Macromolecules* **44**, 444–452 (2010).
43. Gao, C., Vo, C. D., Jin, Y. Z., Li, W. & Armes, S. P. Multihydroxy polymer-functionalized carbon nanotubes: synthesis, derivatization, and metal loading. *Macromolecules* **38**, 8634–8648 (2005).
44. Xu, Z. & Gao, C. Graphene in macroscopic order: liquid crystals and wet-spun fibers. *Acc. Chem. Res.* doi:10.1021/ar4002813 (2014).

Acknowledgements

This work is supported by the National Natural Science Foundation of China (no. 51173162 and no. 21325417), Qianjiang Talent Foundation of Zhejiang Province (no. 2010R10021), Fundamental Research Funds for the Central Universities (no. 2013XZZX003) and Zhejiang Provincial Natural Science Foundation of China (no. R4110175).

Author contributions

L.K. and C.G. conceived and designed the research, analysed the experimental data and wrote the paper; C.G. supervised and directed the project. T.H., B.Z., Y.H., X.Z., K.G. and H.S. contributed to some experiments and took part in discussions.

Additional information

Supplementary Information accompanies this paper at <http://www.nature.com/naturecommunications>

Competing financial interests: The authors declare no competing financial interests.

Reprints and permission information is available online at <http://npng.nature.com/reprintsandpermissions/>

How to cite this article: Kou, L. *et al.* Coaxial wet-spun yarn supercapacitors for high-energy density and safe wearable electronics. *Nat. Commun.* **5**:3754 doi: 10.1038/ncomms4754 (2014).



This work is licensed under a Creative Commons Attribution-NonCommercial-NoDerivs 3.0 Unported License. The images or other third party material in this article are included in the article's Creative Commons license, unless indicated otherwise in the credit line; if the material is not included under the Creative Commons license, users will need to obtain permission from the license holder to reproduce the material. To view a copy of this license, visit <http://creativecommons.org/licenses/by-nc-nd/3.0/>